

Charge Ordering and Ferroelectricity in Half-doped Manganites

Kunihiko Yamauchi¹ and Silvia Picozzi²

1. ISIR-SANKEN, Osaka University, 8-1 Mihogaoka, Ibaraki, Osaka, 567-0047, Japan

2. Consiglio Nazionale delle Ricerche (CNR-SPIN), 67100 L'Aquila, Italy

(Dated: October 17, 2018)

By means of density-functional simulations for half-doped manganites, such as pseudocubic $\text{Pr}_{0.5}\text{Ca}_{0.5}\text{MnO}_3$ and bilayer $\text{PrCa}_2\text{Mn}_2\text{O}_7$, we discuss the occurrence of ferroelectricity and we explore its crucial relation to the crystal structure and to peculiar charge/spin/orbital ordering effects. In pseudocubic $\text{Pr}_{0.5}\text{Ca}_{0.5}\text{MnO}_3$, ferroelectricity is induced in the Zener polaron type structure, where Mn ions are dimerized. In marked contrast, in bilayer $\text{PrCa}_2\text{Mn}_2\text{O}_7$, it is the displacements of apical oxygens bonded to either Mn^{3+} or Mn^{4+} ions that play a key role in the rising of ferroelectricity. Importantly, local dipoles due to apical oxygens are also intimately linked to charge and orbital ordering patterns in MnO_2 planes, which in turn contribute to polarization. Finally, an important outcome of our work consists in proposing Born effective charges as a valid mean to quantify charge disproportionation effects, in terms of anisotropy and size of electronic clouds around Mn ions.

PACS numbers: 75.85.+t, 75.47.Lx, 71.15.Mb

Introduction. “Improper multiferroics”[1], materials where ferroelectricity is driven by either spin ordering (SO), charge ordering (CO) or orbital ordering (OO), constitute a playground for the physics of cross-correlation: the coupling between the different orderings and structural distortions is indeed much stronger and richer than in conventional covalency-driven ferroelectrics.[2] Recently, a complex mechanism of ferroelectricity driven by SO and CO has been proposed both in *half-doped* manganites and in nickelates, supported by theoretical studies.[3–5] In such systems, it is considered that slightly charge-diportionated two magnetic ions form dimers via double exchange interaction, resulting in electric dipoles.[6] In the particular case of bilayer-manganite $\text{Pr}(\text{Sr}_{0.1}\text{Ca}_{0.9})_2\text{Mn}_2\text{O}_7$, it has been experimentally suggested that the transition between two different CO phases is accompanied by the rotation of orbital stripes, in turn related to ferroelectricity.[7]

This letter is meant to provide insights into cross-correlation phenomena and the ferroelectric instability in half-doped manganites via first-principles approaches. Along these lines, there are two delicate problems casted by previous DFT studies: *i*) it is difficult to unambiguously identify the ground state[4, 8, 9] between two different types of atomic (and related electronic) arrangements: *a*) centrosymmetric checkerboard (CB) CO pattern of Mn^{3+} ($t_{2g}^3 e_g^1$) and Mn^{4+} ($t_{2g}^3 e_g^0$) ions and *b*) ferroelectric-active “Zener polaron” (ZP) structure, where the two equivalent $\text{Mn}^{3.5+}$ ions are dimerized via a “bond-centered” charge; *ii*) in the CB structure, the “local charge” of Mn^{3+} and Mn^{4+} ions is in general ill defined [10] and a negligible charge separation (in contrast with the nominal valence difference of $1e$) is often obtained. Here, we address these two problems by reporting our DFT results on pseudocubic $\text{Pr}_{0.5}\text{Ca}_{0.5}\text{MnO}_3$ (PCMO) and bilayer $\text{PrCa}_2\text{Mn}_2\text{O}_7$.

Half-doped manganites: phenomenology. In PCMO, as

in many half-doped manganites, the MnO_2 layer shows the CE-type AFM configuration, consisting of double zigzag FM chains antiferromagnetically coupled both in-plane and out-of-plane, which also invokes CO in the form of Mn^{3+} and Mn^{4+} ions, arranged in a checkerboard pattern, below $T_{\text{CO}}=245\text{K}$ (much higher than the magnetic transition temperature $T_{\text{N}}=175\text{K}$). Between T_{N} and T_{CO} , there is no long-range magnetic ordering, but likely a persisting spin-fluctuating behaviour; we remark, however, that the system remains insulating in the presence of CO. Non-bonding t_{2g} electrons give rise to a localized spin, $S = \frac{3}{2}$, responsible for the AFM super-exchange coupling, whereas e_g orbitals, strongly hybridizing with O $2p$ orbitals and consequently producing broad bands, are responsible for the double exchange mechanism. The half-filled e_g^\uparrow subband is a typical example of the cooperative Jahn-Teller (JT) effect, where the JT distortion of MnO_6 octahedrons results in opening of the gap in the $e_{g\uparrow}$ band and in an insulating ground state. The crystal structure changes symmetry from $Pbnm$ (at room temperature) to lower symmetry in the CO phase, with two possibilities: CB-like centrosymmetric $Pbnm$ (alternatively, $P2_1/m$) and ZP-like polar $P2_1nm$ at low temperature. The stability of these phases and the ferroelectric/dielectric properties are discussed later. We took CD (charge-disordered) $Pbnm$ structure from Ref.[11], and ZP-CO $P2_1nm$ structure from Ref.[12], consistent with previous DFT studies. [9]

In bilayer-manganite $\text{Pr}(\text{Sr}_{0.1}\text{Ca}_{0.9})_2\text{Mn}_2\text{O}_7$ as well, the MnO bilayer shows the CE-type AFM configuration, with peculiar different CO transitions. Upon cooling, the system was shown to undergo two transitions at $T_{\text{CO1}} \sim 370\text{K}$ and at $T_{\text{CO2}} \sim 310\text{K}$ (while $T_{\text{N}} \sim 153\text{K}$), where the system shows a transition from CD phase to the “CO1” phase, forming $\text{Mn}-e_g$ orbital chains along the b -axis, and then to the “CO2” phase, forming orbital chains along the a -axis (which requires

a 90° rotation of the OO pattern, cfr Fig.1). Interestingly, the orbital rotation occurred concomitantly with a rearrangement of Mn³⁺/Mn⁴⁺ cations, leading to a different stacking of the CO-pattern between the bilayers. Although second-harmonic-generation measurements revealed a non-centrosymmetric state[13], ferroelectric/pyroelectric current measurements could not be carried out due to leakage problems. Though truly remarkable, the study of Tokunaga *et al.* leaves many open questions (which will be addressed in this paper), such as how large the polarization is, if and how the polarization is coupled to the SO, CO, and OO, the role of correlation effects vs structural effects, etc.

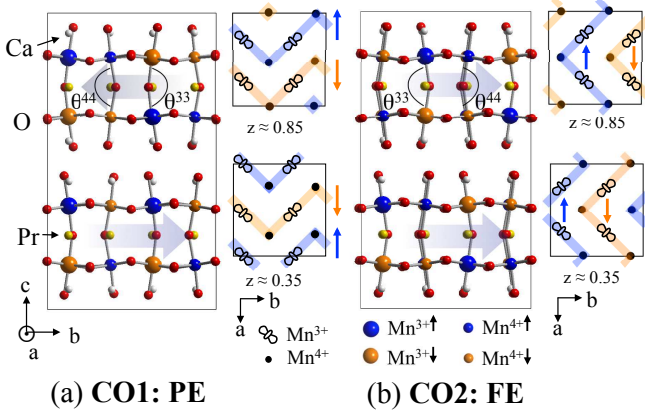


FIG. 1: CO/OO patterns in (a) CO1 phase, with CO stripes running along a , OO zigzag lines along b and in (b) CO2 phase, with CO stripes running along b , OO zigzag lines along a , in bilayer $\text{PrCa}_2\text{Mn}_2\text{O}_7$. Inside each bilayer, the inter-layer coupling is AFM. The Mn-(apical O)-Mn angle is denoted by θ^{33} (θ^{44}) between Mn³⁺ (Mn⁴⁺) ions. The blue arrows indicate the direction of electric dipole moment caused by the difference between θ^{33} and θ^{44} .

Computational details. DFT simulations were performed using the VASP 5.2 code[14] and the PAW pseudopotentials [15] within the GGA+ U formalism[16] ($U=3$ eV and $J=0$ eV for Mn d -states[17]; other values of U are also tested). \mathbf{K} -point meshes of (3, 3, 2) and (2, 2, 1) were used for the Brillouin zone integration for PCMO and $\text{PrCa}_2\text{Mn}_2\text{O}_7$. For the A-site ordering, we consider interlayer Ca-Pr-Ca sandwich stacking along the a -direction for PCMO (to do this, the $Pbnm$ symmetry is kept) and Ca-Pr-Ca sandwich along the c -direction for $\text{PrCa}_2\text{Mn}_2\text{O}_7$. The Sr doping was neglected, since it is expected not to be relevant for our discussion. *i.e.* the one that simultaneously optimizes the energy gain deriving from structural/orbital/spin degrees of freedom. We succeeded in stabilizing all the CO patterns in the insulating state, even with $U=0$.

Born effective charges and charge disproportionation. In PCMO, when considering the CE-AFM configuration and the reduction of symmetry from the CD phase into the CB phase, Mn sites split into Mn³⁺ and Mn⁴⁺ sites;

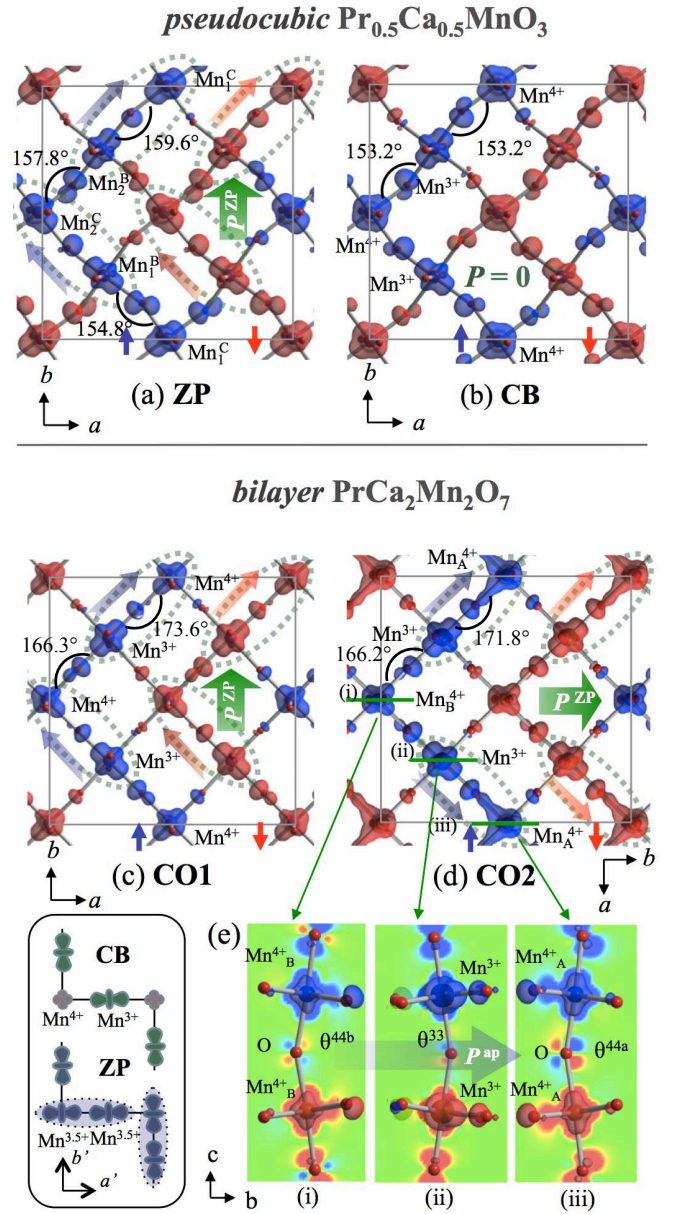


FIG. 2: An isosurface and sections in ab plane of spin density (blue:up, red:down) of Mn- e_g^1 occupied state at (a) ZP and (b) CB in PCMO ($z \approx 0$) and at (c) and (d) at CO1 and (d) at CO2 phases in $\text{PrCa}_2\text{Mn}_2\text{O}_7$ ($z \approx 0.85$). Note the ab frame is shifted and rotated for a better comparison. The direction of local polarization P and of asymmetric e_g electron hopping from Mn³⁺ to Mn⁴⁺ sites are shown by translucent arrows. (e) The same isosurface and the section of CO2, cut in the bc plane. Inset; Schematic picture of CB and ZP orbital patterns. Dimerized Mn ions are surrounded by dotted ellipses.

on the other hand, in the ZP phase, the two original Mn sites (Mn₁ and Mn₂), each split into corner and bridge sites along the spin chain (e.g. Mn₁^C and Mn₁^B), where Mn₁ and Mn₂ ions are dimerized. When comparing the local charge of two different Mn sites, obtained by integrating the charge density within atomic spheres, the charge separation is smaller than 0.01 e , whereas we quan-

tified difference of the local spin moment between Mn^{3+} and Mn^{4+} ions as $0.04\mu_B$ and $0.33\mu_B$ in the ZP and CB phases, respectively. In both cases, such tiny differences (in contrast to the nominal values of $1e$) are affected by large uncertainties, since they depend on the choice of the input radii within which the charge/spin density is integrated. Due to the strong double-exchange nature of Mn- e_g electrons [18], the Mn- d charge is more like “bond-centered” rather than “site-centered”, so that the on-site charge based on an ionic picture is ill defined. Luo *et al.* proposed the Mn- d orbital occupancy as an appropriate indicator of charge separation, giving $\Delta n=0.17e$ in electron-doped CaMnO_3 . [17] Actually, the difference between Mn^{3+} and Mn^{4+} sites in the CB phase is clearly seen in the occupied orbital shape, shown in Fig.2. We go one step further by observing that the topology (size and anisotropy) of the orbitals should be described by “tensorial” instead of “scalar” quantities. Therefore, here we introduce the Born effective charge (BEC), $Z_{\alpha\beta}^* = \delta P_\alpha / \delta u_\beta$ ($\alpha, \beta = x, y, z$) for each ionic displacement u . The diagonalization of Z^* leads to eigenvalues $Z_{x',y',z'}^d$ and eigenvectors, which correspond to the direction of the response of charge density around an ionic site upon displacement. This represents a practical way to characterize the anisotropic nature of pd hybridization along Mn-O bonds. For example, the Mn^{3+} ion in CB phase shows

$$Z_{\text{Mn}^{3+}}^* = \begin{pmatrix} 3.67 & 2.94 & 0.61 \\ 2.38 & 4.89 & 1.48 \\ -0.51 & -0.27 & 4.53 \end{pmatrix} \text{ with } Z_{\text{Mn}^{3+}}^d = \begin{pmatrix} 7.91 \\ 1.20 \\ 3.91 \end{pmatrix},$$

where the first (second) component of Z^d is parallel (perpendicular) to the $3z^2-r^2$ orbital lobe in MnO_2 planes and the third component parallel to the c axis (Fig.2 inset). This clearly reflects the bonding nature of Mn e_g electrons along the spin chain, consistent with the plot of the spin-density (up- minus down-spin components of charge density) reported in Fig.2; the BEC is enhanced along the direction where Mn states shows strong pd hybridization with neighbouring O p -states. On the other hand, the Mn^{4+} ion in the CB phase shows more isotropic Z_d components almost parallel to the (a, b, c) axes (cfr Tab.I). In the ZP phase, we got anisotropic (i.e. Mn^{3+} -type) Z^d both at Mn_1 and Mn_2 sites.

Results: energetics and ferroelectricity. As shown in Tab.II, the total energy in $\text{Pr}_{0.5}\text{Ca}_{0.5}\text{MnO}_3$ shows $E_{\text{CB}} > E_{\text{ZP}}$ (with the experimental structure), as consistent with previous DFT study.[9] The calculated polarization (in Tab. II) shows a small a component, $P_a = -3.3\mu\text{C}/\text{cm}^2$, and a large b component, $P_b = 5.7\mu\text{C}/\text{cm}^2$, originating from two different origins as reported in Ref.[9]. The P_a originates from the dimerization of Mn ions along the orbital stripes (coexistence of bond- and site-centered CO mechanisms, as proposed in Ref.[3]), consistent with the derivation from point charge model; $P_a^{\text{PCM}} = -2.1\mu\text{C}/\text{cm}^2$. The dimerization is reflected by the experimental structure: along

TABLE I: Diagonalized Born effective charge Z^d (e) at Mn sites. Subscripts denote the direction; a' and b' are parallel to diagonal axis, $(a \pm b)/2$, as bonding and non-bonding direction, respectively.

PCMO		ZP	
CB		ZP	
Mn^{3+}	(7.9 $_{a'}$ 1.2 $_{b'}$ 3.9 $_c$)	Mn_1^{B}	(8.4 $_{a'}$ 0.5 $_{b'}$ 4.8 $_c$)
Mn^{4+}	(3.1 $_a$ 5.1 $_b$ 5.8 $_c$)	Mn_2^{B}	(9.5 $_{a'}$ 0.5 $_{b'}$ 4.3 $_c$)
		Mn_1^{C}	(7.2 $_{a'}$ 1.8 $_{b'}$ 4.2 $_c$)
		Mn_2^{C}	(7.3 $_{a'}$ 3.7 $_{b'}$ 3.1 $_c$)
PrCa ₂ Mn ₂ O ₇		CO2	
CO1		CO2	
Mn^{3+}	(6.74 $_x$ 0.89 $_y$ 3.78 $_c$)	Mn^{3+}	(6.29 $_x$ 1.38 $_y$ 3.71 $_c$)
Mn^{4+}	(5.28 $_x$ 3.94 $_y$ 3.45 $_c$)	Mn_A^{4+}	(4.67 $_a$ 4.93 $_b$ 3.49 $_c$)
		Mn_B^{4+}	(4.22 $_a$ 4.28 $_b$ 3.90 $_c$)

the spin chains, the Mn-O-Mn bond angle is modulated by large and small angles, 159.6° (intra-dimer Mn) and $154.8/157.8^\circ$ (inter-dimer Mn). Considering that the large Mn-O-Mn bond angle enhances the double-exchange coupling, we expect the gravity center of charge to shift towards the middle of Mn-Mn dimers rather than being located on Mn sites, resulting in a local electric dipole, suggested as the origin of improper ferroelectricity in $\text{La}_{0.5}\text{Ca}_{0.5}\text{MnO}_3$ [4].

On the other hand, the P_b component is due to artificially imposing the CE-AFM on top of the $P2_1nm$ crystal structure which leads $P_b=0$ in nonmagnetic configuration. When forcing the CE-AFM order, the different interaction between parallel/anti-parallel spin sites causes a Heisenberg-exchange-driven polarization of purely electronic nature.

TABLE II: Total energy difference, $\Delta E^1 = E_{\text{ZP}} - E_{\text{CB}}$ and $\Delta E^2 = E_{\text{CO2}} - E_{\text{CO1}}$ (meV/Mn) for PCMO and $\text{PrCa}_2\text{Mn}_2\text{O}_7$ with different values of U (eV). The polarization P^{tot} ($\mu\text{C}/\text{cm}^2$) is also reported.

PCMO			PrCa ₂ Mn ₂ O ₇		
U	ΔE^1	P^{tot}	U	ΔE^2	P^{tot}
0	-51.7	(-3.56, 5.01, 0)	0	-43.4	(0, 2.18, 0)
3	-59.3	(-3.28, 5.66, 0)	3	-47.2	(0, 1.80, 0)
5	-50.9	(-3.18, 6.06, 0)	5	-48.7	(0, 1.55, 0)

Ferroelectricity in bilayer manganites. In $\text{PrCa}_2\text{Mn}_2\text{O}_7$, the calculated energy (Tab. II) shows that the CO2 phase is energetically lower than CO1, irrespective of the chosen value of U . The calculated P in CO2 phase has a non-zero and sizable y component, $P_y^{\text{Berry}} = 1.8\mu\text{C}/\text{cm}^2$. As already pointed out in Ref.[13], the FE polarization is related to the stacking pattern of the CO bilayers. As shown in Fig. 1, the GdFeO_3 -like tilting of MnO_6 octahedron largely displaces apical O (O^{ap}) ions away from the bond center along the b direction. One expects the displacement of O^{ap} ion to be suppressed by an elastic contribution, when Mn- e_g electrons form strong Mn- O^{ap} -Mn bonding along

TABLE III: Mn-O^{ap}-Mn angle θ ($^\circ$) in CD, CO1, and CO2 phases.

	θ^{33}	θ^{44}
CD	162.80	162.80
CO1	166.41	159.22
CO2	162.91	162.63(A), 159.28(B)

the c direction. Indeed, the Mn-O^{ap}-Mn bond angles θ , summarized in Tab. III, reveal $\theta^{44} < \theta^{33}$, i.e. O^{ap} ion is more displaced between Mn⁴⁺ ions, with respect to the one between Mn³⁺ ions. The coupling between the O^{ap} displacement and the staggered GdFeO₃-tilting pattern causes a local dipole inside the bilayer; the latter cancels out with the nearby bilayer in the CO1 phase (resulting in antiferroelectricity), whereas it gives rise to a net P in the CO2 phase.

Furthermore, we observe that the polarization value in CO2 is close to the P calculated by using PCM $P_y^{\text{PCM}}(\text{CD})=1.9 \mu\text{C}/\text{cm}^2$, considering all Mn^{3.5+} with homogeneous valence and $P_y^{\text{PCM}}(\text{CO})=1.8 \mu\text{C}/\text{cm}^2$, considering Mn³⁺/Mn⁴⁺ mixed valences. The almost identical value of $P_y^{\text{PCM}}(\text{CD})$ and $P_y^{\text{PCM}}(\text{CO})$ shows that the origin of P lies in the apical O ion displacement, and is not crucially dependent on the Mn³⁺/Mn⁴⁺ CO pattern *per se*. In addition, this marks a clear difference with respect to purely CO-induced ferroelectricity, occurring for example in Fe₃O₄ and in iron-based fluorides.[19, 20]

Further insights can be gained by looking at the electronic structure. The OO both in the CO1 and CO2 phases can be clearly seen in the spin-density plot reported in Fig.2, showing a similarity between CO1 and ZP, and between CO2 and CB phase in PCMO, respectively (Fig.2). In analogy with ZP, CO1 shows a dimerization between Mn ions so as to induce polarization in the MnO₂ plane; however, the net induced polarization is canceled out by inter-layer antiferroelectric stacking. The difference of CO2 with respect to CB is represented by two different Mn⁴⁺ sites, namely Mn_A⁴⁺ and Mn_B⁴⁺, and by the anisotropic orbital shape. A careful look at the spin density plot reveals the anisotropy of the e_g electron hopping. In the CO2 phase, the charge on the Mn_A⁴⁺ site shows a polar behaviour, slightly deviated from x^2-y^2 orbital shape, elongated and pointing toward one of the neighboring Mn³⁺ sites. This is consistent with the dimerization of Mn ions, as present in the experimental structure, *i.e.* the larger angle of Mn³⁺-O-Mn_A⁴⁺ than of Mn³⁺-O-Mn_B⁴⁺ indicated in Fig. 2. Although the ZP state is realized thanks to the double-exchange nature of Mn e_g electrons, here the dimerization seems to be induced by an external factor, *i.e.* the effective electric field induced by O^{ap} displacements. The spin-density plot in the bc plane, shown in Fig. 2(e), reveals the lobes of Mn charge pointing along the c direction, forming the inter-layer

Mn-O-Mn bonding. Remarkably, in both CO phases, Mn ions form dimers so as to induce a local P^{ZP} in MnO₂ planes, that cooperatively adds to the local P^{ap} caused by the apical O^{ap} displacement, showing an enhancement of the total P . By using the calculated BEC tensors, the local contributions to P from each layer can be calculated separately and given by the summation of the product of the BEC (Z^*) by the relevant ionic displacement. We therefore obtained $P_y(\text{CaO}^{\text{ap}})=-0.36\mu\text{C}/\text{cm}^2$, $P_y(\text{PrO}^{\text{ap}})=P^{\text{ap}}=0.65\mu\text{C}/\text{cm}^2$, and $P_y(\text{MnO}_2^{\text{ip}})=P^{\text{ZP}}=0.71\mu\text{C}/\text{cm}^2$ per layer, whereas the total $P_b=1.8\mu\text{C}/\text{cm}^2$. This notably shows that the polarization, P^{ap} and P^{ZP} , originating from different mechanisms and different ions, give quantitatively similar contributions. The clear difference in the mechanism driving ferroelectricity between PCMO and PrCa₂Mn₂O₇ appear in Z^{d} (Tbl. I): all Mn ions show a strongly *anisotropic* Z^{d} along dimers in the ZP phase, whereas *isotropic* Z^{d} of Mn⁴⁺ is obtained in the CO2 phase. This implies that in PrCa₂Mn₂O₇ the e_g double exchange mechanism is not relevant but rather structural effects play a role in the ferroelectricity.

Conclusions. We have investigated the ferroelectric half-doped manganites and have made a comparison between pseudo-cubic PCMO and bilayer PrCa₂Mn₂O₇. In PCMO, although there is an arbitrariness in the crystal structure (which was proposed to be either polar or not), a polarization is expected in the ZP structure. In bilayer PrCa₂Mn₂O₇, the intercalation of layers gives rise to a peculiar situation, where both the Mn dimerization process and the apical oxygen displacements contribute to ferroelectric polarization, predicted to be of the order of several $\mu\text{C}/\text{cm}^2$. We finally note BEC tensor is a good measure to quantify CO and OO in manganites.

Acknowledgments. KY thanks Y. Taguchi, Y. Tokunaga and D. Okuyama for fruitful discussions and acknowledges kind hospitality at CNR-SPIN L'Aquila, where the manuscript was written. The research leading to these results received funding from the European Research Council under the European Community 7th Framework Programme FP7 (2007-2013)/ERC Grant Agreement no. 203523 and from JST-CREST "Creation of Innovative Functions of Intelligent Materials on the Basis of the Element Strategy". Some figures are plotted using the program VESTA[21].

-
- [1] M. Mostovoy and S.W. Cheong *Nature Mater* **6**, 13 (2007).
 - [2] S. Picozzi, and C. Ederer, *J. Phys.: Cond. Mat.* **21**, 303201 (2009).
 - [3] D.V. Efremov, J. van der Brink, D. I. Khomskii, *Nat. Mater.* **3**, 853 (2004).
 - [4] G. Giovannetti, S. Kumar, J. van den Brink, S. Picozzi, *Phys. Rev. Lett.* **103**, 037601 (2009).

- [5] G. Giovannetti, S. Kumar, D. Khomskii, S. Picozzi, J. van den Brink, Phys. Rev. Lett. **103**, 156401 (2009).
- [6] D. V. Efremov, J. van den Brink, and D. Khomskii, Nature Mater. **12**, 856 (2004).
- [7] Y. Tokunaga et al., Nature Mater. **5**, 937 (2006).
- [8] C. H. Patterson, Phys. Rev. B **72** 085125 (2005).
- [9] G. Colizzi, A. Filippetti, and V. Fiorentini, Phys. Rev. B **82** 140101(R) (2010).
- [10] W. Luo et al., Phys. Rev. Lett. **99**, 036402 (2007).
- [11] Z. Jirák et al., J. M. M. M. **53**, 153 (1985).
- [12] A. Daoud-Aladine, J. Rodriguez-Carvajal, L. Pinsard-Gaudart, M.T. Fernandez-Diaz, A. Revcolevschi, Phys. Rev. Lett. **89**, 097205 (2002).
- [13] H. Itoh, et al., Appl. Phys. Lett. **96**, 032902 (2010).
- [14] G. Kresse and J. Furthmüller, Phys. Rev. B **54**, 11169 (1996).
- [15] P. E. Blöchl, Phys. Rev. B **50**, 17953 (1994).
- [16] V.I. Anisimov, F. Aryasetiawan and A.I. Lichtenstein, J. Phys.: Cond. Mat. **9**, 767 (1997).
- [17] Weidong Luo, et. al, Phys. Rev. Lett. **99**, 036402 (2007).
- [18] V. I. Anisimov, I. S. Elfimov, and M. A. Korotin, K. Terakura, Phys. Rev. B. **55**, 15494 (1997).
- [19] K. Yamauchi, T. Fukushima, S. Picozzi, Phys. Rev. B **79**, 212404 (2009).
- [20] K. Yamauchi and S. Picozzi, Phys. Rev. Lett. **105**, 107202 (2010).
- [21] K. Momma and F. Izumi, J. Appl. Crystallogr., **41**, 653 (2008).